Accepted Manuscript

Implicit finite volume simulation of 2D shallow water flows in flexible meshes

J. Fernández-Pato, M. Morales-Hernández, P. García-Navarro

Please cite this article as: J. Fernández-Pato, M. Morales-Hernández, P. García-Navarro, Implicit finite volume simulation of 2D shallow water flows in flexible meshes, *Comput. Methods Appl. Mech. Engrg.* (2017), http://dx.doi.org/10.1016/j.cma.2017.08.050

This is a PDF file of an unedited manuscript that has been accepted for publication. As a service to our customers we are providing this early version of the manuscript. The manuscript will undergo copyediting, typesetting, and review of the resulting proof before it is published in its final form. Please note that during the production process errors may be discovered which could affect the content, and all legal disclaimers that apply to the journal pertain.

Implicit finite volume simulation of 2D shallow water flows in flexible meshes

J. Fernández-Pato[a,*], M. Morales-Hernández[a], P. García-Navarro[a],

[a]*LIFTEC-CSIC, University of Zaragoza, Spain*

Abstract

In this work, an implicit method for solving 2D hyperbolic systems of equations is presented, focusing on the application to the 2D shallow water equations. It is based on the first order Roe's scheme, in the framework of finite volume methods. A conservative linearization is done for the flux terms, leading to a non-structured matrix for unstructured meshes thus requiring iterative methods for solving the system. The validation is done by comparing numerical and exact solutions in both unsteady and steady cases. In order to test the applicability of the implicit scheme to real world situations, a laboratory scale tsunami simulation is carried out and compared to the experimental data. The implicit schemes have the advantage of the unconditional stability, but a quality loss in the transient solution can appear for high CFL numbers. The properties of the scheme are well suited for the simulation of unsteady shallow water flows over irregular topography using all kind of meshes.

Key words: Finite volumes, Shallow-water equations, Implicit schemes, Unstructured meshes, Efficiency analysis

1. Introduction

In computational fluid dynamics, the non-linearity of the governing equations combined with the usually huge number of cells and thence unknowns in a complex problem

*Corresponding author: Tel.: +34 876555057; fax: +34 976761882. Ed. Torres Quevedo, María de Luna 3, CP 50018, Zaragoza. Spain.
  Email addresses: `jfpato@unizar.es` (J. Fernández-Pato)

implies a large amount of computing effort and time. There is an interest in developing efficient numerical methods. In general terms, numerical schemes used to solve time dependent problems can be classified in two groups, attending to the time evaluation of the unknowns: explicit and implicit methods.

Explicit schemes update the solution at every cell from the known values of the system at the current time, whereas implicit schemes generate a system of N equations with N unknowns, being N the number of computational cells multiplied by the number of variables to solve for each cell. Explicit schemes are restricted by numerical stability reasons.

The advantage of using implicit schemes is that they are, in theory, unconditionally stable, even though they may be less accurate than explicit schemes for unsteady flows when using large time step sizes. A compromise is required between stability gain and accuracy loss on the results. Traditionally (Yee et al., 1985; Anderson, 1995; Toro, 1999), this constitutes the main reason for using implicit methods in steady state computations. In these of problems, the accuracy loss during the transient state is not so important and the possibility of choosing a larger time step for the simulation often allows the faster calculation of the steady state.

There is a wide range of applications of implicit methods within the field of computational hydraulics. Some simplified overland flow models have been applied in combination with an implicit numerical scheme (Lal, 1998a,b; Lal and Toth, 2013; Fernández-Pato and García-Navarro, 2016a,b). For example, the Zero-Inertia (ZI) simplification of the Shallow Water Equations (SWE), often termed as Diffusion Wave, has been reported as inefficient when discretized by means of an explicit scheme compared to the implicit ZI model (Fernández-Pato and García-Navarro, 2016a,b) or even the full SWE (Cea et al., 2010; Wang et al., 2011; López-Barrera et al., 2012).

In order to maximize the simulation efficiency, some authors have applied implicit methods to SWE for solving 1D problems e.g. channels, pipes or river flow (Burguete and García-Navarro, 2004; García-Navarro et al., 1994) and 2D problems (Casoulli, 1990; Krn et al., 2011; Li and Duffy, 2012; J. and Das, 2013; Tavelli and Dumbser,

2

2014; Kesserwani and Liang, 2015), showing the possibility of simulating with large time step sizes. ADCIRC is a model (Luettich and Westerink, 1991) that solves the reformulated shallow water equations. The continuity equation is used in the form of the so-called Generalized Wave Continuity equation (GWCE). In this solver, the GWCE can be treated semi-implicitly or explicitly in time whereas a temporal discretization of the momentum equations is based on a semi-implicit scheme. On the other hand, CLAWPACK (LeVeque, 1997) uses a finite volume methodology for solving linear and nonlinear hyperbolic systems of conservation laws, but it is restricted to rectangular meshes and uses an explicit discretization.

One of our goals is to develop a 2D model capable of working in any kind of mesh (structured or unstructured), based on an implicit finite volume method and hence taking advantage of: 1) the conservative discretization that is automatically obtained, through the direct use of the integral form of the conservation laws and 2) the unconditional stability inherent to the implicit schemes. Additionally, we aim to implement a robust wet/dry treatment, which is not usually correctly addressed in the implicit models.

One of the most relevant issues when dealing with shallow flows, regardless of the temporal scheme, is the correct treatment of wet/dry fronts in a flood wave advancing over an irregular topography. This is a nontrivial challenge for the development of an accurate numerical scheme, as these situations frequently lead to extreme and nonphysical velocities in the wet/dry front, causing instabilities and a drastic reduction in the numerical time step (Murillo et al., 2007; Burguete et al., 2008). In Medeiros and Hagen (2013) a few techniques used in the last years are classified in four categories: thin film, element removal, depth extrapolation and negative depth. Each group has benefits and drawbacks regarding, for instance, the correct capture of the wet/dry interface or the local and global mass conservation. More recently, Murillo and García-Navarro (2010); Murillo and García-Navarro (2012) presented a novel procedure to deal with wet/dry fronts consisting of the water positivity preserving and the friction losses limitation. This is the strategy considered in the present work.

The main goal of this research is to formulate a robust and well-balanced 2D implicit

numerical scheme in order to solve both transient and steady flows, but specially focused in the last ones. Unstructured meshes are used in order to get a better fitting of irregular geometries, such as the curvature of a river meander or a steep mountain catchment. The wetting and drying procedure is tested by means of several test cases.

2. 2D scalar non-linear equations

As starting point, let us consider a generic non-linear bidimensional scalar equation:

$$\frac{\partial u}{\partial t} + \nabla \mathbf{f} = 0, \qquad \mathbf{f} = (f_x, f_y), \qquad \mathbf{a} = (a_x, a_y) = \frac{d\mathbf{f}}{du} \tag{1}$$

where $\mathbf{a}$ represents the wave speed vector and u and $\mathbf{f}$ are the conserved variable and its flux, respectively.

2.1. Numerical model

By considering a control volume Ω (area in 2D) and by integrating (1) assuming a fixed-in-time control volume:

$$\frac{d}{dt} \int_\Omega u d\Omega + \int_\Omega \nabla \mathbf{f} d\Omega = 0 \tag{2}$$

Invoking Gauss' theorem:

$$\frac{d}{dt} \int_\Omega u d\Omega + \int_{\partial\Omega} (\mathbf{f} \cdot \mathbf{n}) \partial\Omega = 0 \tag{3}$$

where $\mathbf{n}$ is the outward-pointing normal vector to the surface $\partial\Omega$.

Considering the control volume Ω of area S_i with N_w polygonal faces of length l_w, each with an outward-pointing normal vector n_w (see Figure 1) and assuming a piecewise constant representation, Eq. (3) can be written in a discrete form

$$\frac{u_i^{n+1} - u_i^n}{\Delta t} S_i + \sum_{j,w=1}^{N_w} (\delta \mathbf{f} \cdot \mathbf{n})_w^- l_w = 0 \tag{4}$$

4

where superscript n indicates the time level and:

$$(\delta \mathbf{f} \cdot \mathbf{n})_w^- = (\tilde{\mathbf{a}} \cdot \mathbf{n})_w^- \delta u_w \tag{5}$$

where $\delta u_w = u_j - u_i$ with u_i and u_j being the cell average values of the variable u at two adjacent cells, and $\tilde{\mathbf{a}}_w = \frac{\mathbf{f}_j - \mathbf{f}_i}{u_j - u_i}$ is the average advection speed at the cell edge.

[Figure 1 about here.]

Note that, following the upwind philosophy, only the in-coming components of the information (-) are taken into account in Eq. (4). The temporal discretization can be done in terms of a weight θ to select a fully-implicit ($\theta = 1$) or a fully-explicit method ($\theta = 0$):

$$\frac{u_i^{n+1} - u_i^n}{\Delta t} S_i + \theta \sum_{j,w=1}^{N_w} \left[(\delta \mathbf{f} \cdot \mathbf{n})_w^- \right]^{n+1} l_w + (1-\theta) \sum_{j,w=1}^{N_w} \left[(\delta \mathbf{f} \cdot \mathbf{n})_w^- \right]^n l_w = 0 \tag{6}$$

The fluxes at $n+1$ time need to be linearized as follows (Burguete and García-Navarro, 2004):

$$\delta \mathbf{f}_w^{n+1} \simeq \delta \mathbf{f}_w^n + \mathbf{a}_j^n \Delta u_j - \mathbf{a}_i^n \Delta u_i \tag{7}$$

where $\Delta u_i = u_i^{n+1} - u_i^n$ and $\Delta u_j = u_j^{n+1} - u_j^n$. Note that the advection speeds are evaluated at the cell centers in (7).

Therefore, projecting on the normal-pointing direction the ingoing component of the flux:

$$\left[(\delta \mathbf{f} \cdot \mathbf{n})_w^- \right]^{n+1} \simeq \left[(\delta \mathbf{f} \cdot \mathbf{n})_w^- \right]^n + \left(\mathbf{a}_j^n \cdot \mathbf{n}_w \right)^- \Delta u_j - \left(\mathbf{a}_i^n \cdot \mathbf{n}_w \right)^- \Delta u_i \tag{8}$$

By replacing (8) in (6):

5

$$\Delta u_i - \theta \frac{\Delta t}{S_i} \sum_{j,w=1}^{N_w} (\mathbf{a}_i^n \cdot \mathbf{n}_w)^- l_w \Delta u_i + \theta \frac{\Delta t}{S_i} \sum_{j,w=1}^{N_w} \left(\mathbf{a}_j^n \cdot \mathbf{n}_w\right)^- l_w \Delta u_j = -\frac{\Delta t}{S_i} \sum_{j,w=1}^{N_w} \left[(\delta \mathbf{f} \cdot \mathbf{n})_w^-\right]^n l_w \tag{9}$$

Finally, by reordering in a compact coefficient scheme:

$$a_i \Delta u_i + \sum_{j,w=1}^{N_w} b_w \Delta u_j = k_i \tag{10}$$

where

$$a_i = 1 - \theta \frac{\Delta t}{S_i} \sum_{j,w=1}^{N_w} (\mathbf{a}_i^n \cdot \mathbf{n}_w)^- l_w,$$

$$b_w = \theta \frac{\Delta t}{S_i} \left(\mathbf{a}_j^n \cdot \mathbf{n}_w\right)^- l_w$$

$$k_i = -\frac{\Delta t}{S_i} \sum_{j,w=1}^{N_w} (\tilde{\mathbf{a}}^n \cdot \mathbf{n})_w^- \delta u_w^n l_w$$

2.2. Stability condition

For 1D explicit numerical schemes, the time step is chosen for ensuring the no-interaction among the other outward waves from the neighbour Riemann problems, taking into account the wave speed and the half-length of the cell $\Delta x/2$. However, the process is more complicated for 2D problems, specially if the spatial discretization is done by means of unstructured meshes. Let us define the equivalent distance to Δx:

$$\Delta x_i' = \frac{S_i}{\max_{1,N_w}(l_w)} \tag{11}$$

where S_i represents the cell area and l_w is the face length (see Figure 1). When using an explicit scheme, the limited time step for each face is given by:

$$\Delta t_{i,w} = \frac{\min(\Delta x_i', \Delta x_j')}{\max(|\tilde{\mathbf{a}}_w \cdot \mathbf{n}|)} \tag{12}$$

6

The stability is given by the traditional Courant-Friedrich-Levy (CFL) number, given by:

$$\Delta t = \text{CFL} \min_{Mesh}(\Delta t_{i,w}) \tag{13}$$

or

$$\text{CFL} = \frac{\Delta t}{\min_{Mesh}(\Delta t_{i,w})} \tag{14}$$

where $\min_{Mesh}(\Delta t_{i,w})$ represents the minimum $\Delta t_{i,w}$ value along the whole computational mesh.

In case of using structured 2D meshes, the maximum CFL number for the explicit scheme is $1/2$, whereas CFL=1 is allowed for some unstructured triangular meshes. On the other hand, implicit schemes benefit of theoretical unconditional stability. Hence, CFL number becomes a multiplicative factor of the maximum time step allowed by the explicit scheme for stability reasons. The present work is intended to explore this issue.

2.3. Test case: 2D inviscid Burgers' equation

Let us consider the 2D inviscid Burgers' equation:

$$\frac{\partial u}{\partial t} + \nabla \mathbf{f} = 0, \qquad \mathbf{f} = \left(\frac{u^2}{2}, \frac{u^2}{2}\right) \tag{15}$$

The problem setup consists of a bidimensional Riemann problem proposed in Barley (1988). Figure 2 shows the initial conditions and the analytical solution at $t = 9s$. A 3600 cell structured square mesh is used for the spatial discretization. Figure 3 shows the numerical solution for explicit and implicit methods at $t = 9s$. As seen on this figure, the numerical solution provided by the implicit scheme trends to be more diffusive than the corresponding to the explicit scheme, specially when choosing CFL>1.

7

[Figure 2 about here.]

[Figure 3 about here.]

3. 2D system of equations: application to Shallow Water equations

The general conservative formulation for a system in 2D is:

$$\frac{\partial \mathbf{U}}{\partial t} + \frac{\partial \mathbf{F}(\mathbf{U})}{\partial x} + \frac{\partial \mathbf{G}(\mathbf{U})}{\partial y} = \mathbf{S}(\mathbf{U}, x, y) \tag{16}$$

or

$$\frac{\partial \mathbf{U}}{\partial t} + \nabla \cdot \mathbf{E} = \mathbf{S} \tag{17}$$

being $\mathbf{E} = (\mathbf{F}, \mathbf{G})$.

The existence of a Jacobian matrix of the system is the basis of the upwind numerical discretization and it is defined by:

$$\mathbf{J}_n = \frac{\partial \mathbf{E} \cdot \mathbf{n}}{\partial \mathbf{U}} = \frac{\partial \mathbf{F}}{\partial \mathbf{U}} n_x + \frac{\partial \mathbf{G}}{\partial \mathbf{U}} n_y \tag{18}$$

being $\mathbf{E} \cdot \mathbf{n}$ the flux normal to a direction given by the unit vector normal to cell $\mathbf{n} = (n_x, n_y)$. The numerical model is developed under the hypothesis that the problem is dominated by advection and is strongly determined by the source terms.

3.1. Numerical model

The upwind finite volume philosophy, when adapted to conservation laws with source terms, helps to formulate well-balanced schemes by means of a unified formulation of the flux derivatives and source terms as reported in Murillo and García-Navarro (2010); García-Navarro and Vázquez-Cendón (2000):

8

$$\frac{d}{dt}\int_\Omega \mathbf{U}d\Omega + \int_\Omega (\mathbf{\nabla}\cdot\mathbf{E})d\Omega = \int_\Omega \mathbf{S}d\Omega \Rightarrow \frac{d}{dt}\int_\Omega \mathbf{U}d\Omega + \sum_{j,w=1}^{N_w}(\delta\mathbf{E}\cdot\mathbf{n})_w^- l_w = \sum_{j,w=1}^{N_w}\mathbf{S}_w^- l_w \quad (19)$$

The focus in (19) is put on the flux and source terms contributions defined at the grid edges w. The difference in vector $\mathbf{U}$ across the grid edge and the source term can be projected onto the matrix eigenvectors basis, as follows:

$$\delta\mathbf{U}_w = \tilde{\mathbf{P}}_w\mathbf{A}_w, \qquad \mathbf{S}_w = \tilde{\mathbf{P}}_w\mathbf{B}_w \quad (20)$$

being $\mathbf{A}$ and $\mathbf{B}$ the wave and source strength vectors, given by:

$$\mathbf{A}_w = (\alpha^1,\alpha^2,\alpha^3)_w^T, \qquad \mathbf{B}_w = (\beta^1,\beta^2,\beta^3)_w^T \quad (21)$$

Then, the flux and source terms in (19) can be expressed as follows:

$$\delta(\mathbf{E}\cdot\mathbf{n})_w = \mathbf{J}_n\delta\mathbf{U}_w = \sum_{m=1}^{3}(\tilde{\lambda}\alpha\tilde{\mathbf{e}})_w^m, \qquad \mathbf{S}_w = \sum_{m=1}^{3}(\beta\tilde{\mathbf{e}})_w^m \quad (22)$$

Hence:

$$\frac{\Delta\mathbf{U}_i}{\Delta t}S_i + \sum_{j,w=1}^{N_w}(\delta\mathbf{E}\cdot\mathbf{n})_w^- l_w = \sum_{j,w=1}^{N_w}\mathbf{S}_w^- l_w \quad (23)$$

A fundamental point in the recent literature has been to get schemes that satisfy the preservation of steady-states such as still water equilibrium in shallow water system. The difficulty to build such schemes was pointed out by several authors and led to the notion of well-balanced schemes or Property-C (García-Navarro and Vázquez-Cendón, 2000). The explicit implementation of the above scheme has proved to be well-balanced not only in cases of water at rest but also in moving water steady state situations (Murillo and García-Navarro, 2010). According to that work, numerical experimentation proves that careless discretization of resistance may lead to a wrong equilibrium in

9

steady state and to oversize and inadequate values for the discrete friction forces, specially in wet/dry fronts that can interfere with the stability of the numerical solution. The upwind unified treatment of all terms, including boundary shear stress, ensures Property-C even in steady cases with non-zero velocity (Murillo and García-Navarro, 2012).

In the search of an implicit formulation of the scheme, the time evaluation of the flux terms in (23) is done by means of the implicitness parameter θ:

$$\frac{\Delta \mathbf{U}_i}{\Delta t} S_i + \theta \sum_{j,w=1}^{N_w} \left[(\delta \mathbf{E} \cdot \mathbf{n})_w^- \right]^{n+1} l_w + (1-\theta) \sum_{j,w=1}^{N_w} \left[(\delta \mathbf{E} \cdot \mathbf{n})_w^- \right]^n l_w = \sum_{j,w=1}^{N_w} \left(\mathbf{S}_w^- \right)^n l_w \quad (24)$$

with a linearization for the fluxes given by Burguete and García-Navarro (2004):

$$(\delta \mathbf{E} \cdot \mathbf{n})_w^{n+1} \approx (\delta \mathbf{E} \cdot \mathbf{n})_w^n + \mathbf{J}_{n,w} \Delta \mathbf{U}_j - \mathbf{J}_{n,w} \Delta \mathbf{U}_i \quad (25)$$

Note that the source terms have been discretized explicitly.

By replacing (25) in (24), upwinding the Jacobian and reordering:

$$\mathbf{aa}_i \Delta \mathbf{U}_i + \sum_{j,w=1}^{N_w} \mathbf{bb}_w \Delta \mathbf{U}_j = \mathbf{k}_i \quad (26)$$

with

$$\mathbf{aa}_i = \mathbf{I} - \theta \frac{\Delta t}{S_i} \sum_{w=1}^{N_w} \left(\mathbf{J}_{n,w}^- \right)^n l_w \quad (27)$$

$$\mathbf{bb}_w = \theta \frac{\Delta t}{S_i} \left(\mathbf{J}_{n,w}^- \right)^n l_w \quad (28)$$

$$\mathbf{k}_i = -\frac{\Delta t}{S_i} \sum_{w=1}^{N_w} \left[(\delta \mathbf{E} \cdot \mathbf{n})_w^- \right]^n l_w + \frac{\Delta t}{S_i} \sum_{w=1}^{N_w} \left(\mathbf{S}_w^- \right)^n l_w \quad (29)$$

Expressions (26) to (29) represent a system of equations conforming a $3N_{cells} \times 3N_{cells}$ matrix built in terms of 3×3 block matrices as follows:

10

$$\tilde{\mathbf{A}}\mathbf{X} = \mathbf{k} \tag{30}$$

The linear system (30) needs to be solved by means of a matrix inversion technique. For unstructured triangular meshes, this results in a $3N_{cells} \times 3N_{cells}$ block matrix:

$$\begin{pmatrix} \mathbf{aa}_1 & & \mathbf{bb}_w & & \mathbf{bb}_w & & \mathbf{bb}_w \\ \mathbf{bb}_w & \mathbf{aa}_2 & & \mathbf{bb}_w & \mathbf{bb}_w & & \\ & \mathbf{bb}_w & \mathbf{aa}_3 & & & \mathbf{bb}_w & \mathbf{bb}_w \\ & & & \ddots & & & \\ & & & & \ddots & & \\ & \mathbf{bb}_w & \mathbf{bb}_w & \mathbf{bb}_w & & \mathbf{aa}_{N-1} & \\ \mathbf{bb}_w & & \mathbf{bb}_w & & \mathbf{bb}_w & & \mathbf{aa}_N \end{pmatrix} \begin{pmatrix} \Delta\mathbf{U}_1 \\ \Delta\mathbf{U}_2 \\ \Delta\mathbf{U}_3 \\ \vdots \\ \vdots \\ \Delta\mathbf{U}_{N-1} \\ \Delta\mathbf{U}_N \end{pmatrix} = \begin{pmatrix} \mathbf{k}_1 \\ \mathbf{k}_2 \\ \mathbf{k}_3 \\ \vdots \\ \vdots \\ \mathbf{k}_{N-1} \\ \mathbf{k}_N \end{pmatrix} \tag{31}$$

In this work, the Biconjugate Gradient Stabilized (BiCGStab) linear matrix solver (van der Vorst, 1992; Guennebaud et al., 2010) has been used. It has been combined with an efficient ILUT preconditioner (Saad, 1994) in order in improve the convergence rate. This linear solver takes a great advantage of the use of the sparse storage for the matrix, avoiding the storage of the null elements. This reduces the computation time and the memory usage, which is an important issue due to the huge size of the matrix and the quadratic increase of the memory usage with the computational grid size.

3.2. Application to 2D Shallow Water equations

The 2D Shallow Water equations conforms a hyperbolic non-linear system that can be written as in (16), where:

$$\mathbf{U} = (h, q_x, q_y)^T, \qquad q_x = hu, \qquad q_y = hv \tag{32}$$

$$\mathbf{F} = \left(q_x, \frac{q_x^2}{h} + \frac{1}{2}gh^2, \frac{q_x q_y}{h} \right)^T, \qquad \mathbf{G} = \left(q_y, \frac{q_x q_y}{h}, \frac{q_y^2}{h} + \frac{1}{2}gh^2 \right)^T \tag{33}$$

$$\mathbf{S} = (0, gh(S_{0x} - S_{fx}), gh(S_{0y} - S_{fy}))^T \tag{34}$$

11

with h representing the water depth and (u,v) the depth-averaged components of the velocity vector along the (x,y) coordinates.

The slope terms are

$$S_{0x} = -\frac{\partial z}{\partial x}, \quad S_{0y} = -\frac{\partial z}{\partial y} \tag{35}$$

and the friction-associated loses in terms of the Manning roughness number n are:

$$S_{fx} = \frac{n^2 u \sqrt{u^2 + v^2}}{h^{4/3}}, \quad S_{fy} = \frac{n^2 v \sqrt{u^2 + v^2}}{h^{4/3}} \tag{36}$$

The Jacobian matrix of the flux in the normal-pointing direction is:

$$\mathbf{J}_n = \frac{\partial \mathbf{E} \cdot \mathbf{n}}{\partial \mathbf{U}} = \mathbf{A}n_x + \mathbf{B}n_y \tag{37}$$

where

$$\mathbf{A} = \frac{\partial \mathbf{F}}{\partial \mathbf{U}} = \begin{pmatrix} 0 & 1 & 0 \\ c^2 - u^2 & 2u & 0 \\ -uv & v & u \end{pmatrix}, \qquad \mathbf{B} = \frac{\partial \mathbf{G}}{\partial \mathbf{U}} = \begin{pmatrix} 0 & 0 & 1 \\ -uv & v & u \\ c^2 - v^2 & 0 & 2v \end{pmatrix} \tag{38}$$

in terms of the flow velocities and the surface wave speed $c = \sqrt{gh}$. Then:

$$\mathbf{J}_n = \begin{pmatrix} 0 & n_x & n_y \\ -u(\mathbf{u} \cdot \mathbf{n}) + c^2 n_x & \mathbf{u} \cdot \mathbf{n} + u n_x & u n_y \\ -v(\mathbf{u} \cdot \mathbf{n}) + c^2 n_y & v n_x & \mathbf{u} \cdot \mathbf{n} + v n_y \end{pmatrix} \tag{39}$$

The eigenvalues and eigenvectors are given by:

$$\lambda^1 = \mathbf{u} \cdot \mathbf{n} - c, \qquad \lambda^2 = \mathbf{u} \cdot \mathbf{n}, \qquad \lambda^3 = \mathbf{u} \cdot \mathbf{n} + c \tag{40}$$

$$\mathbf{e}^1 = \begin{pmatrix} 1 \\ u - cn_x \\ v - cn_y \end{pmatrix}, \qquad \mathbf{e}^2 = \begin{pmatrix} 0 \\ -cn_y \\ cn_x \end{pmatrix}, \qquad \mathbf{e}^3 = \begin{pmatrix} 1 \\ u + cn_x \\ v + cn_y \end{pmatrix} \tag{41}$$

The matrices that diagonalize the Jacobian are:

$$\mathbf{P} = (\mathbf{e}^1, \mathbf{e}^2, \mathbf{e}^3) = \begin{pmatrix} 1 & 0 & 1 \\ u - cn_x & -cn_y & u + cn_x \\ v - cn_y & cn_x & v + cn_y \end{pmatrix} \tag{42}$$

$$\mathbf{P}^{-1} = -\frac{1}{2c} \begin{pmatrix} -\mathbf{u} \cdot \mathbf{n} - c & n_x & n_y \\ 2(vn_x - un_y) & 2n_y & -2n_x \\ \mathbf{u} \cdot \mathbf{n} - c & -n_x & -n_y \end{pmatrix} \tag{43}$$

$$\mathbf{J}_n = \mathbf{P}\mathbf{\Lambda}\mathbf{P}^{-1}, \qquad \mathbf{P}^{-1}\mathbf{J}_n\mathbf{P} = \mathbf{\Lambda}, \qquad \mathbf{\Lambda} = \begin{pmatrix} \lambda^1 & 0 & 0 \\ 0 & \lambda^2 & 0 \\ 0 & 0 & \lambda^3 \end{pmatrix} \tag{44}$$

The approximate Jacobian $\mathbf{J}_{n,w}$ of the system together with the source and wave strengths are constructed in terms of the averaged variables, corresponding to Roe's approximate Riemann solver (Roe, 1981):

$$\tilde{u}_w = \frac{u_i\sqrt{h_i} + u_j\sqrt{h_j}}{\sqrt{h_i} + \sqrt{h_j}}, \qquad \tilde{v}_w = \frac{v_i\sqrt{h_i} + v_j\sqrt{h_j}}{\sqrt{h_i} + \sqrt{h_j}}, \qquad \tilde{c}_w = \sqrt{g\frac{h_i + h_j}{2}} \tag{45}$$

This results in the next eigenvalues and eigenvectors:

$$\tilde{\lambda}_w^1 = (\tilde{\mathbf{u}} \cdot \mathbf{n} + \tilde{c})_w, \qquad \tilde{\lambda}_w^2 = (\tilde{\mathbf{u}} \cdot \mathbf{n})_w, \qquad \tilde{\lambda}_w^3 = (\tilde{\mathbf{u}} \cdot \mathbf{n} - \tilde{c})_w \tag{46}$$

$$\tilde{\mathbf{e}}_w^1 = \begin{pmatrix} 1 \\ \tilde{u} + \tilde{c}n_x \\ \tilde{v} + \tilde{c}n_y \end{pmatrix}_w, \qquad \tilde{\mathbf{e}}_w^2 = \begin{pmatrix} 0 \\ -\tilde{c}n_y \\ \tilde{c}n_x \end{pmatrix}_w, \qquad \tilde{\mathbf{e}}_w^3 = \begin{pmatrix} 1 \\ \tilde{u} - \tilde{c}n_x \\ \tilde{v} - \tilde{c}n_y \end{pmatrix}_w \tag{47}$$

The wave strengths α and source strengths β coefficients in (21) are given by:

13

$$\alpha_w^{1,3} = \frac{\delta h_w}{2} \mp \frac{1}{2\tilde{c}_w}[\delta(hu)n_x + \delta(hv)n_y - \tilde{\mathbf{u}} \cdot \mathbf{n}\delta h]_w = \frac{\delta h_w}{2} \mp \frac{1}{2\tilde{c}_w}(\delta\mathbf{q}_w - \tilde{\mathbf{u}}_w\delta h_w)\mathbf{n} \quad (48)$$

$$\alpha_w^2 = \frac{1}{\tilde{c}_w}[(\delta(hv) - \tilde{v}\delta h)n_x - (\delta(hu) - \tilde{u}\delta h)n_y]_w \quad (49)$$

$$\beta_w^1 = -\frac{1}{2}\tilde{c}_w\left(\delta z + S_f d_n\right)_w = -\beta_w^3, \qquad \beta_w^2 = 0 \quad (50)$$

The magnitude d_n is the normal distance between neighbour centers and $S_{f,w}$ represents the discrete energy grade line for the bidimensional case (Murillo and García-Navarro, 2010):

$$S_{f,w} = \frac{\tilde{n}_w^2\tilde{\mathbf{u}} \cdot \mathbf{n}\,|\tilde{\mathbf{u}}|}{\max{(h_i, h_j)}^{4/3}} \quad (51)$$

being

$$\tilde{n}_w = \frac{1}{2}\left(n_i + n_j\right) \quad (52)$$

the average Manning's roughness coefficient at the interface w.

Finally, by applying an upwind treatment to the fluxes and source terms:

$$\tilde{\lambda}_w^{\pm,m} = \frac{1}{2}(\tilde{\lambda} \pm |\tilde{\lambda}|)_w^m \quad (53)$$

$$\beta_w^{1-,3-} = \frac{1}{2}\beta_w^{1,3}[1 - sign(\tilde{\lambda}_w^{1,3})], \qquad \beta_w^2 = 0 \quad (54)$$

3.3. Source terms limitation and wet/dry treatment

In the last decades, the effort has been put on an upwind discretization as well as a good balance between source terms and fluxes (García-Navarro and Vázquez-Cendón,

14

2000). However, this is not enough when dealing with realistic scenarios where bed slope or friction terms play a dominant role over convective terms and unrealistic non-physical solutions such as negative values of water depth can appear due to the wrong estimation of the source amount. In those cases, one option is reducing the time step size until the positivity is guaranteed or the non-physical solutions are removed. The main drawback of this strategy is that the time step size may be decreased in many orders of magnitude hence rising the number of time steps done, and consequently the time needed to compute the solution. Therefore, a good philosophy could be to adopt a correct estimation of the source amount instead of reducing the time step size.

In this work, the strategy followed in Murillo and García-Navarro (2010) for an explicit Godunov finite volume scheme is adapted for the implicit scheme presented. First the discrete friction terms are limited avoiding them to change the sign of the velocity within one time step. By splitting them into a sum of two components β_S^m (bed slope) and β_F^m (friction)

$$\beta^m = \beta_S^m + \beta_F^m, \qquad m = 1, 2, 3. \tag{55}$$

it is feasible to define the following quantities coming from the Riemann Problem between cells i and j at edge w:

$$q_i^* = (hu_i + \alpha^1 \tilde{\mathbf{e}}_2^1)n_x + (hv_i + \alpha^1 \tilde{\mathbf{e}}_3^1)n_y - \beta_S^1 - \beta_F^1$$
$$q_i^\triangledown = (hu_i + \alpha^1 \tilde{\mathbf{e}}_2^1)n_x + (hv_i + \alpha^1 \tilde{\mathbf{e}}_3^1)n_y - \beta_S^1 \tag{56}$$

In case that $q_i^\triangledown q_i^* < 0$ the effect of friction terms is overestimated to the extent that flow could move back, resulting in an impossible situation. Accordingly, the friction terms should be redefined as:

$$\beta_F^1 = \begin{cases} q_i^\triangledown & \text{if} & q_i^\triangledown q_i^* < 0 \\ \beta_F^1 & \text{otherwise} \end{cases}, \qquad \beta_F^3 = -\beta_F^1 \tag{57}$$

in order to preserve the sign of the discharge.

15

Additionally, negative values in the water depth can appear due to the wrong estimation of linearized source terms β^m in subcritical flow (Murillo and García-Navarro, 2010). In order to avoid this undesirable situation, the following quantities can be defined with the aim of limiting the source terms amount:

$$
h_i^* = h_i^n + \left(\alpha^1 - \frac{\beta^1}{\tilde{\lambda}^1} \right)_w \geq 0, \qquad h_j^{**} = h_j^n - \left(\alpha^2 - \frac{\beta^2}{\tilde{\lambda}^2} \right)_w \geq 0
$$
$$
\beta_{min}^1 = (h_i^n + \alpha^1)\tilde{\lambda}^1, \qquad \beta_{min}^2 = (-h_j^n + \alpha^2)\tilde{\lambda}^2
\tag{58}
$$

Therefore:

- If $h_i^* < 0$ and $h_j^{**} > 0$, β^1 is redefined not only to ensure conservation, i.e., $\beta^2 = -\beta^1$ but also a non-negative value h_j^{**}:

$$
\beta^1 = \begin{cases} \beta_{min}^1 & \text{if} & -\beta_{min}^1 \geq \beta_{min}^2 \\ \beta^1 & \text{otherwise} \end{cases}, \qquad \beta^2 = -\beta^1
\tag{59}
$$

- If $h_i^* > 0$ and $h_j^{**} < 0$, β^2 is also redefined:

$$
\beta^2 = \begin{cases} \beta_{min}^2 & \text{if} & -\beta_{min}^2 \geq \beta_{min}^1 \\ \beta^2 & \text{otherwise} \end{cases}, \qquad \beta^1 = -\beta^2
\tag{60}
$$

These cheap and simple corrections when discretizing the source terms allow to build robust solutions recovering the conventional CFL condition, avoiding large reductions in the time step size to ensure positivity solutions (Murillo and García-Navarro, 2012). The well-balanced property is ensured by a the proper discretization of the explicit part in **k**.

3.4. Time step size

As in the 2D scalar case (Section 2.2), the time step is dynamically chosen as follows:

$$
\Delta t = \text{CFL} \min_{Mesh}(\Delta t_{i,w})
\tag{61}
$$

where

$$\Delta t_{i,w} = \frac{\min(\Delta x_i', \Delta x_j')}{\max_{m=1,2,3}(|\tilde{\lambda}_w^m|)}, \qquad \Delta x_i' = \frac{S_i}{max_{1,N_w}(l_w)} \tag{62}$$

Therefore, the CFL number becomes a multiplicative factor of the maximum time step allowed by the explicit scheme. The present formulation follows closely the results in Murillo and García-Navarro (2010) where the influence of the source terms was controlled by means of the augmented Riemann solver.

3.5. Boundary conditions

Apart from the internal elements, it is necessary to formulate adequately several boundary conditions in order to model properly any physical situation. In this paper, four different boundary conditions are used: closed boundaries, h-fixed, Q-fixed and free outflow.

Closed boundaries are solid walls that completely block the water flow. When a closed boundary is considered, the model sets zero normal flow across the boundary, but allows tangential velocities (see Figure 4, left).

[Figure 4 about here.]

In order to impose fixed values of the water depth h, the boundary value h_{fixed} is set as the new value for the boundary cell iB at time $n+1$ (see Figure 4, center), as follows:

$$h_{iB}^{n+1} = h_{fixed} \tag{63}$$

On free outflow boundary conditions (see Figure 4, right), the model calculates water depths and unit discharges applying the full equations from the internal cells. Hence, no condition is imposed on these nodes. This should be equivalent to assuming that spatial derivatives of water level $(h + z)$ and velocities are equal to zero.

17

The imposed inlet water discharge Q (Figure 4, center) needs to be converted to unit discharge x and y components, $q_x = hu$ and $q_y = hv$, respectively, by dividing by the inlet segment length L_{inlet} and taking into account the inlet direction (see Figure 5), as follows:

$$q_x = \frac{Q}{L_{inlet}} \cos \varphi, \qquad q_y = \frac{Q}{L_{inlet}} \sin \varphi \qquad (64)$$

[Figure 5 about here.]

4. Mesh sensitivity analysis

In this section, a simple test case is presented in order to show the benefits of triangular unstructured meshes (TU), in terms of its adaptability to irregular topography, which is the most usual in natural environments, as river catchments.

This test presents a comparison between TU and rectangular structured (RS) meshes with approximately the same number of cells (~ 1500) in a $50m \times 30m$ domain with three bed irregularities, a square obstacle and two spherical humps (see Figure 6). Both computational meshes are shown in Figure 7. A constant Manning's roughness value of $0.03sm^{-1/3}$ and dry initial conditions ($h = 0m$) are assumed for the entire domain. All the boundaries are closed except the left one in which a constant water depth of $h = 0.3m$ is imposed. It should be noted that the TU mesh offers the possibility of performing a local refinement in the areas of interest. In this test case, the refinement is done in the spherical humps in order to obtain a good discretization of the topography.

Figure 8 shows the evolution of the water depth h at $t = 3s$, $t = 9s$ and $t = 600s$ for both RS and TU meshes. The unstructured and locally-refined mesh shows a better fit to the rounded topography with the same number of cells in both transient and steady states. Hence, it is the most suitable choice when dealing with irregular beds. In this numerical example, the good behaviour of the implicit scheme under both transient and steady wet/dry fronts is also verified (8). The numerical scheme is capable of solving this phenomenology without noticing any issues.

18

[Figure 6 about here.]

[Figure 7 about here.]

[Figure 8 about here.]

5. Test cases

5.1. Water at rest

The motivation for this first test case is to check the preservation of the C-property of the model and thence if the source terms are well-balanced in still water situations. The bed level is given by:

$$z(x, y) = \max \left\{ 0, 2000 - 0.00032 \left[(x - 4000)^2 + (y - 4000)^2 \right] \right\} \quad (65)$$

The initial quiescent water level is set in $1000m$. The $8000m \times 8000m$ domain has been discretized by means of a 5000 cells unstructured triangular mesh. The simulation has been run for $600s$ with CFL numbers of 2 and 50, leading to time steps of $1.05s$ and $26.2s$, respectively, without observing significant differences. Figure 9 shows the three-dimensional representation of the steady state and the cross-sectional plot of the solution at the final time.

[Figure 9 about here.]

5.2. Transcritical steady state over a bump

This test case proposed in Murillo and García-Navarro (2012) leads to a final steady state by which the implicit method accuracy can be evaluated. The case setup consists of a horizontal bed level with a bump given by $z(8 \le x \le 12) = 0.2 - 0.05(x - 10)^2$. The channel length and width are 25 m and 1.5 m, respectively. As initial condition, a uniform water level of 0.5 m is imposed. The boundary conditions consists of a fixed

19

water input discharge upstream ($hu = 1.53m^2/s$) and free flow downstream. CFL numbers up to 75 can be chosen for reaching the steady state. Figure 10 shows the comparison between numerical and exact solution for this case with CFL=50. Figure 11 shows the temporal evolution of the numerical results for different times until the steady state with CFL=2.

[Figure 10 about here.]

[Figure 11 about here.]

In order to evaluate the quality of the steady numerical solutions, the L_1 error is computed for several CFL numbers. Table 1 and Figure 12 show the error values in terms of the CFL. In the light of the results, it is clear that the implicit scheme provides a very good steady solution for high CFL numbers.

[Table 1 about here.]

[Figure 12 about here.]

5.3. MacDonald test case

Let us consider now a case that was first proposed by MacDonald in MacDonald (1996) and MacDonald et al. (1997). It represents a 1D configuration for open channel flow in which an analytical solution can be obtained for the steady state. The test consists of a rectangular channel $150m$ long with an irregular bed level. A constant Manning friction coefficient of $0.03s/m^{1/3}$ is set all over the channel. A constant discharge of $20m^3/s$ is imposed as inlet boundary condition and a fixed water depth of $0.800054m$ is set in the outlet. The analytical solution for the water depth along the channel is given by:

$$h(x) = 0.71 + 0.25\sin^2\left(\frac{3\pi x}{300}\right) \tag{66}$$

20

Although this case was designed for testing 1D numerical solutions, a 2D configuration is assumed in the present work starting from dry bed initial conditions in order to check the wet/dry algorithm in both transient and steady situations.

Figure 13 shows the comparison between numerical and analytical solutions. A CFL number up to 300 can be reached without observing noticeable changes in the steady solution. As in the previous test case, the L_1 errors are provided, together with the CPU time and the speed-up values, defined as the ratio between the CPU times corresponding to implicit and explicit schemes (Table 2). Figure 14 shows the representation of the CPU computational times and speed-up values for several CFL numbers. The implicit scheme shows a high efficiency in this case by reaching the steady solution up to 12 times faster than the explicit version of the numerical scheme, which requires $100.9s$ to complete the simulation. For the sake of completeness, the graphical representation of the L_1 error is also shown in Figure 15.

[Figure 13 about here.]

[Figure 14 about here.]

[Table 2 about here.]

[Figure 15 about here.]

5.4. Circular dam-break

In order to test the behaviour of the implicit scheme under transient conditions, a circular dam break test is considered in this section. A square frictionless domain of $200m \times 200m$ with no slope is considered. All the boundaries are closed and the initial state for the water depth is given by (see Figure 16):

$$h(x, y, 0) = \begin{cases} 4.0 & \text{if } \sqrt{x^2 + y^2} \leq 100m \\ 1.0 & \text{otherwise} \end{cases} \tag{67}$$

21

Figure 16 also shows the line that will be used to extract a longitudinal plot in where the numerical solutions for several CFL numbers are compared to the exact solution, computed as a 1D solution on the radial direction using a high resolution grid (see Figure 17).

[Figure 16 about here.]

A 10363 cell unstructured triangular mesh is used for the spatial discretization. Figure 17 shows the comparison between exact and numerical solutions for several CFL values at $t = 12s$. In the light if the results, a good agreement between numerical and exact solution is observed. As expected in a transient case, the larger the CFL value the more diffusive the numerical solution becomes. Nevertheless, in this particular case, an acceptable solution is found up to CFL=25.

The computational times and the speed-up values for this test case are shown in Figure 19. In this particular case, the implicit scheme needs a CFL of 50 in order to reach the solution faster than the explicit one, which took $0.69s$. Therefore, an implicit temporal discretization of the SWE is not the most suitable choice for this transient problem due to the diffusion of the numerical solution associated to the large CFL number required to beat the explicit scheme.

Figure 18 shows the comparison for the water depth values among several CFL numbers at $t = 12s$. As in the longitudinal profile, this 2D view shows the diffusion of the solution as the CFL increases, specially noticeable with CFL=50.

In order to perform a mesh convergence study, the L_1 error is computed for this case for all the CFL values using 5 different computational meshes ranging from 1560 to 19389 cells. Table 3 shows the CPU time, speed-up and L_1 error in terms of the CFL number for all the meshes considered for this test case. The CPU times for the first two meshes were negligible and they are not shown. All these data are graphically represented in two ways. Figure 20 shows the L_1 error with respect of CFL number for the 5 meshes. It can be seen that the error asymptotically increases with the CFL value and decreases with the mesh refinement, as expected.

22

On the other hand, Figure 21 shows the results of the mesh convergence study. The L_1 error is plotted against the square root of the number of cells (both axis in log scale) for several CFL values. In all the cases, a convergence of almost order 1 is achieved.

[Figure 17 about here.]

[Figure 18 about here.]

[Figure 19 about here.]

[Table 3 about here.]

[Figure 20 about here.]

[Figure 21 about here.]

Another interesting comparison is performed in this test case. The simulation is repeated by considering an implicit numerical scheme with $\theta = 1/2$ in equations (27) and (28). A 10363 cell mesh is used in this case. Figure 22 shows the longitudinal profiles of the numerical solutions for several CFL values. It can be seen that the solutions become oscillatory for CFL>2. This behaviour agrees with the non-TVD character of this scheme for high CFL numbers (Burguete and García-Navarro, 2004).

Figure 23 shows the comparison between numerical solutions corresponding to $\theta = 1$ and $\theta = 1/2$ for CFL=2 and CFL=10. As expected, the scheme with $\theta = 1/2$ becomes less diffusive than the full implicit one. This is specially noticeable in the rarefaction wave area.

[Figure 22 about here.]

[Figure 23 about here.]

23

5.5. Tsunami test case

In order to test the implicit scheme in extreme transient conditions, a tsunami test case in a 1/400 laboratory scale is carried out in this section (Liu et al., 2008). This case was also reproduced by other authors for testing 1D shallow-water schemes (Burguete et al., 2008) or Large Time Step schemes with CFL>1 (Morales-Hernández et al., 2014). Figure 24 shows the bed elevation map and the gauging points in where experimental data is available. The coordinates for the three gauges are:

$$P1 = (4.52m, 1.196m), \qquad P2 = (4.52m, 1.696m), \qquad P3 = (4.52m, 2.196m) \quad (68)$$

[Figure 24 about here.]

The domain $(5.488m \times 3.388m)$ is discretized by means of a unstructured triangular mesh of 19000 elements. A constant roughness Manning's coefficient of $0.01sm^{-1/3}$ is set and a uniform water level of $h + z = 0.0$ is assumed as initial condition. As in the experimental setup, all the boundaries are closed but the one corresponding to the offshore incoming wave, which is defined as a temporal variation of the water level $(h + z)$, as shown in Figure 25.

[Figure 25 about here.]

The numerical simulation has been carried out using several CFL numbers for the implicit scheme in order to establish a comparison between numerical and experimental results. A 3D representation of the numerical results for water depth at $t = 0$, $t = 5s$, $t = 10s$, $t = 13s$, $t = 18s$, $t = 25s$ is shown in Figure 26 in where a proper solution of all the wet/dry interfaces is reached at any time of the simulation. In order to validate the model, the numerical results for several CFL numbers corresponding to the water level $(h + z)$ are compared with the experimental measures provided by Liu et al. (2008) at the $P1$, $P2$ and $P3$ probes (Figure 27). The numerical results for the explicit scheme are also shown. A good agreement between numerical and experimental

24

results is observed, even for large CFL numbers. When choosing CFL<1, the implicit scheme produces the same solution as the explicit one, ensuring the consistency of the model. As expected, the larger the CFL the more diffusive the implicit numerical solution is, but acceptable results are achieved until CFL=50 for all the considered gauges. The solution for CFL=200 is also shown in order to remark the stability of the implicit numerical model. In this case, the diffusivity of the solution is also due to the resolution loss of the inlet boundary data when choosing large time steps.

Figure 28 shows the CPU times and the speed-up values. In this case, the explicit scheme took $22.26s$ to complete the simulation. An speed-up of 1.14 is obtained when using a CFL of 50 while an speed-up of 2.08 is reached with CFL=200.

[Figure 26 about here.]

[Figure 27 about here.]

[Figure 28 about here.]

6. Conclusions

The implementation of an implicit conservative upwind scheme to both non-linear scalar and systems of equations has been presented in this work, focusing on the application to the 2D shallow water equations. In order to follow a logical procedure, the same numerical scheme has been presented for 2D scalar case and 2D systems of equations case, paying a special attention to the wet/dry front correction algorithm. As the numerical scheme is implicitly discretized in time, a matrix solver is needed in order to solve simultaneously the hydraulic variables for the whole mesh. In this work, this has been done by means of the so called BI-CGSTAB, one of the most efficient iterative methods when sparse storage strategies are used, specially when it is combined with a matrix preconditioner as ILUT.

The model is validated in both smooth-transient and steady situation through several cases with analytical solution. A laboratory scale tsunami case with measured data is

25

also presented for an additional comparison of the numerical results against measured data. In general terms, all the results show a good agreement with the analytical solution or experimental data, even for large CFL numbers (up to 300 in some cases). A quality loss in the transient solution due to the high numerical diffusion is also observed when using large time steps but the steady solution is reached without noticing numerical issues. Hence, in the light of the results presented in this work, the overall conclusions can be summarized in the next points:

- The presented implicit numerical scheme is robust, conservative and preserves well the C-property regardless of the CFL value in quiescent water cases.

- Steady solutions are perfectly reproduced with large CFL numbers, up to 300 in the MacDonald test case presented in Section 5.3. The efficiency of the implicit numerical scheme is remarkable in this case, leading to an speed-up value of 12.

- A good agreement between numerical and exact solution is observed in strong transient cases, as the circular dam break presented in Section 5.4. As expected, the larger the CFL value the more diffusive is the transient solution but acceptable solutions has been found for CFL up to 25 in this particular case. The tsunami test case presented in Section 5.5 also shows a good agreement between numerical solutions and experimental data, even for large CFL numbers. Despite the inherent diffusivity of the implicit transient solutions, the unconditional stability of the model is pointed out in this case.

Despite the fact that an implicit method normally requires less solution steps, each one demands more computational time than the solutions obtained by an explicit scheme. This strongly depends on the number of iterations the matrix solver needs to do for achieving the convergence. Overall, the larger the CFL the more diffusive the implicit numerical solution is. Nevertheless, if the numerical diffusion can be assumable, the possible gain in performance due to the high CFL choice can be a point in favour of using these kind of numerical schemes under transient conditions. On the other hand, the steady solutions are perfectly reached regardless of the CFL value so the implicit methodology is adequate and

26

recommendable for solving the steady or nearly-steady flows.

References

Anderson, J., 1995. Computational fluid dynamics. McGraw-Hill.

Barley, J., 1988. A survey of Operator Splitting Applied to Upwind Differentiating. Numerical Analysis Report 2/88. University of Reading.

Burguete, J., García-Navarro, P., 2004. Implicit schemes with large time step for non-linear equations: application to river flow hydraulics. International Journal for Numerical Methods in Fluids 46, 607–636.

Burguete, J., Garca-Navarro, P., Murillo, J., 2008. Friction term discretization and limitation to preserve stability and conservation in the 1d shallow-water model: Application to unsteady irrigation and river flow. International Journal for Numerical Methods in Fluids 58, 403–425.

Casoulli, V., 1990. Semi-implicit finite difference methods for the two-dimensional shallow water equations. Journal of Computational Physics 86, 56–74.

Cea, L., Garrido, M., Puertas, J., 2010. Experimental validation of two-dimensional depth-averaged models for forecasting rainfall-runoff from precipitation data in urban areas. Journal of Hydrology 382, 88–102.

27

Fernández-Pato, J., García-Navarro, P., 2016a. 2D zero-inertia model for solution of overland flow problems in flexible meshes. Journal of Hydrologic Engineering 21, 04016038.

Fernández-Pato, J., García-Navarro, P., 2016b. Numerical simulation of valley flood using an implicit diffusion wave model. Ingeniería del agua 20, 115 – 126.

García-Navarro, P., Alcrudo, F., Priestley, A., 1994. An implicit method for water flow modelling in channels and pipes. Journal of Hydraulic Research 32, 721–742.

García-Navarro, P., Vázquez-Cendón, M., 2000. On numerical treatment of the source terms in the shallow water equations. Computers & Fluids 29, 951–979.

Guennebaud, G., Jacob, B., et al., 2010. Eigen v3. http://eigen.tuxfamily.org.

J., B., Das, S., 2013. Modeling of shallow-water equations by using implicit higher-order compact scheme with application to dam-break problem. Journal of Applied & Computational Mathematics 2, 132.

Kesserwani, G., Liang, Q., 2015. RKDG2 shallow-water solver on non-uniform grids with local time steps: Application to 1D and 2D hydrodynamics. Applied Mathematical Modelling 39, 1317–1340.

Krn, T., de Brye, B., Gourgue, O., Lambrechts, J., Comblen, R., Legat, V., Deleersnijder, E., 2011. A fully implicit wettingdrying method for dg-fem shallow water models, with an application to the scheldt estuary. Computer Methods in Applied Mechanics and Engineering 200, 509–524.

Lal, Wasantha, A., 1998a. Performance comparison of overland flow. Journal of the Hydraulic Engineering 124, 342–349.

Lal, Wasantha, A., 1998b. Weighted implicit finite-volume model for overland flow. Journal of the Hydraulic Engineering 124, 941–950.

Lal, A.M.W., Toth, G., 2013. Implicit TVDLF methods for diffusion and kinematic flows. Journal of Hydraulic Engineering 139, 974–983.

LeVeque, R., 1997. Wave propagation algorithms for multi-dimensional hyperbolic systems. Journal of Computational Physics 131, 327–353.

Li, S., Duffy, C.J., 2012. Fully-coupled modeling of shallow water flow and pollutant transport on unstructured grids. Procedia Environmental Sciences 13, 2098 – 2121.

Liu, P.F., Yeh, H., Synolakis, C., 2008. Advanced Numerical Models for Simulating Tsunami Waves and Runup. Advances in Coastal and Ocean Engineering. volume 10. World Scientific.

López-Barrera, D., García-Navarro, P., Brufau, P., Burguete, J., 2012. Diffusive-wave based hydrologic-hydraulic model with sediment transport. i: Model development. Journal of Hydrologic Engineering 17, 1093–1104.

Luettich, R., Westerink, J., 1991. A solution for the vertical variation of stress, rather than velocity, in a three-dimensional circulation model. International Journal for Numerical Methods in Fluids 12, 911–928.

MacDonald, I., 1996. Analysis and computation of steady open channel flow. Ph.D. thesis. University of Reading.

MacDonald, I., Baines, M., Nichols, N., Samuels, P., 1997. Analytic benchmark solutions for open-channel flows. Journal of Hydraulic Engineering 123, 1041–1045.

Medeiros, S.C., Hagen, S.C., 2013. Review of wetting and drying algorithms for numerical tidal flow models. International Journal for Numerical Methods in Fluids 71, 473–487.

Morales-Hernández, M., Hubbard, M., García-Navarro, P., 2014. A 2D extension of a Large Time Step explicit scheme (CFL>1) for unsteady problems with wet/dry boundaries. Journal of Computational Physics 263, 303–327.

Murillo, J., García-Navarro, P., 2010. Weak solutions for partial differential equations with source terms: Application to the shallow water equations. Journal of Computational Physics 229, 4327–4368.

Murillo, J., García-Navarro, P., 2012. Augmented versions of the HLL and HLLC Riemann solvers including source terms in one and two dimensions for shallow flow applications. Journal of Computational Physics 231, 6861–6906.

Murillo, J., García-Navarro, P., 2012. Wave Riemann description of friction terms in unsteady shallow flows: Application to water and mud/debris floods. J. Comput. Phys. 231, 1963–2001.

Murillo, J., García-Navarro, P., Burguete, J., Brufau, R., 2007. The influence of source terms on stability, accuracy and conservation in two-dimensional shallow flow simulation using triangular finite volumes. International Journal for Numerical Methods in Fluids 54, 543–590.

Roe, P., 1981. Approximate riemann solvers, parameter vectors, and difference schemes. Journal of Computational Physics 43, 357–372.

Saad, Y., 1994. ILUT: A dual threshold incomplete lu factorization. Numerical Linear Algebra with Applications 1, 387–402.

Tavelli, M., Dumbser, C., 2014. A high order semi-implicit discontinuous galerkin method for the two dimensional shallow water equations on staggered unstructured meshes. Applied Mathematics and Computation 234, 623–644.

Toro, E., 1999. Riemann Solvers and Numerical Methods for Fluid Dynamics: A Practical Introduction. Springer.

van der Vorst, H., 1992. BI-CGSTAB - A fast and smoothly converging variant of BI-CG for the solution of nonsymmetric linear-systems. SIAM Journal on Scientific and Statistical Computing 13, 631–644.

Wang, Y., Liang, Q., Kesserwani, G., Hall, J.W., 2011. A positivity-preserving zero-inertia model for flood simulation. Computers & Fluids 46, 505 – 511. 10th ICFD Conference Series on Numerical Methods for Fluid Dynamics (ICFD 2010).

Yee, H., Warming, R., Harten, A., 1985. Implicit total variation diminishing (TVD) schemes for steady-state calculations. Journal of Computational Physics 57, 327–360.
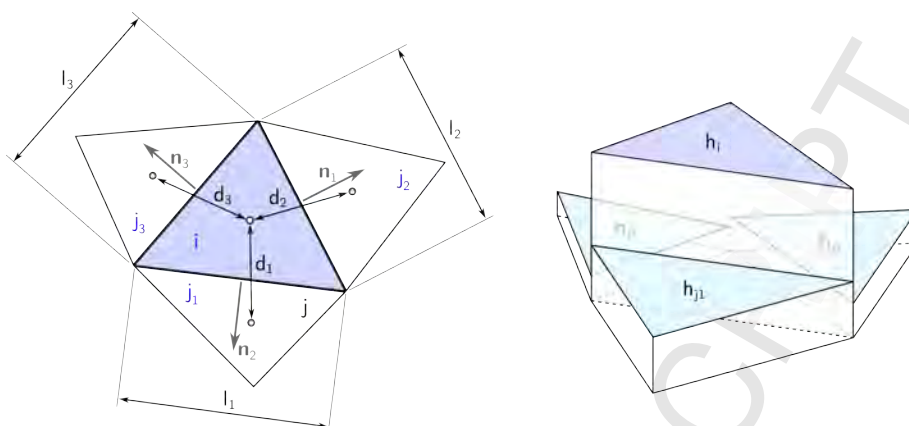
Figure 1: Cell connectivity sketch in a triangular unstructured mesh.
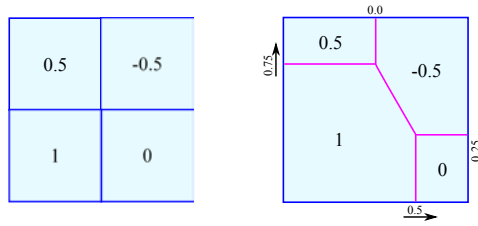
Figure 2: Initial conditions and analytic solution for the 2D Riemann problem at $t = 9s$. The arrows represent the shock speeds of each front.

33
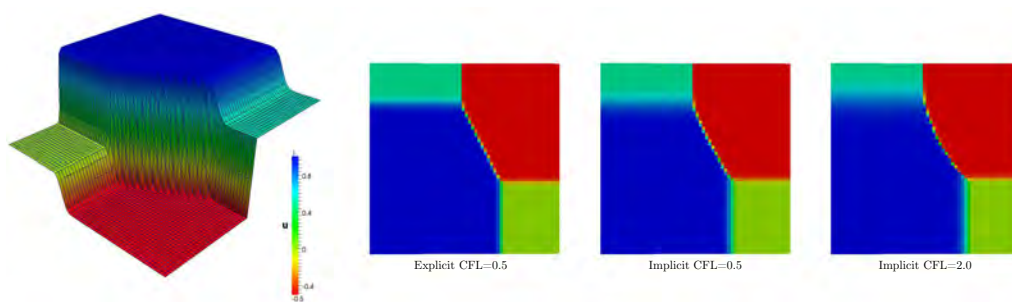
Figure 3: Numerical solutions to the Riemann problem at $t = 9s$.
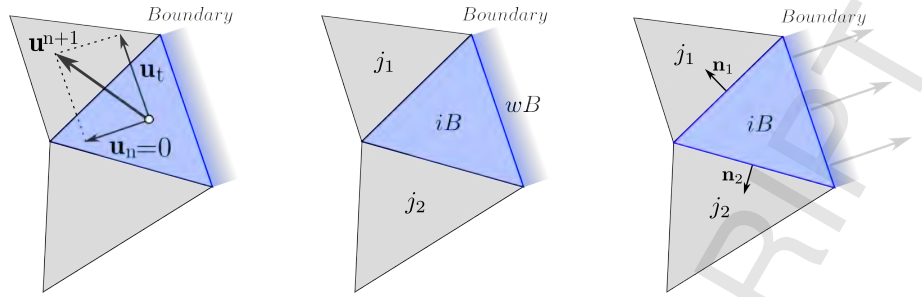
Figure 4: Closed wall (left), fixed (center) and free outflow (right) boundary conditions.
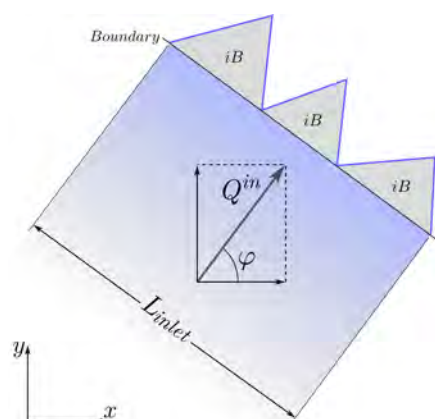
Figure 5: Inlet water discharge boundary condition.

36
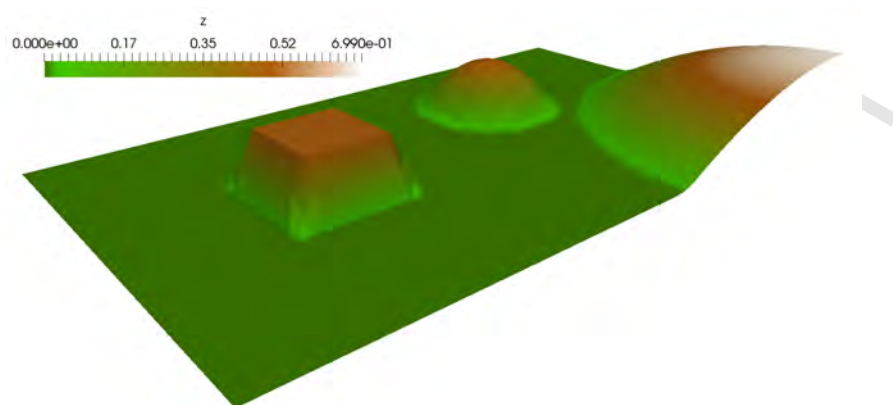
Figure 6: 3D representation of the domain (bed elevation is exaggerated 2 times).

37
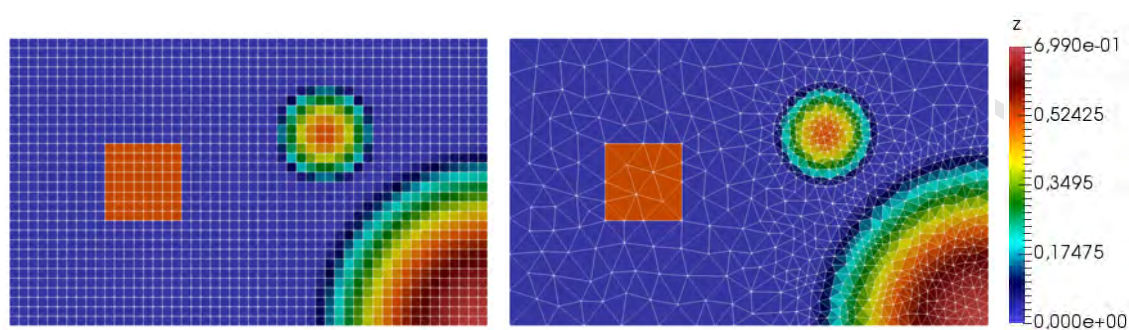
Figure 7: Rectangular structured (left) and triangular unstructured (right) meshes.

38
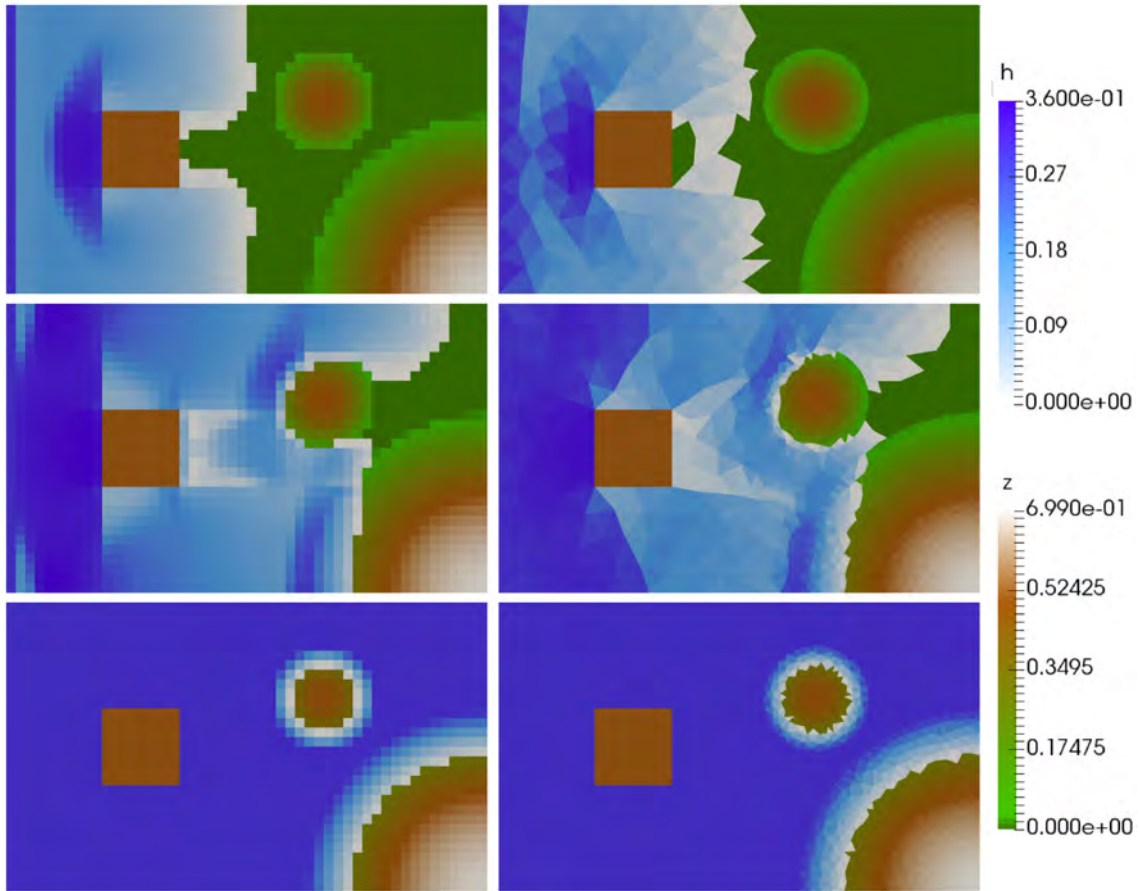
Figure 8: Numerical results for the mesh adaptability study. Water depth at $t = 3s, 9s$ and $600s$.

38
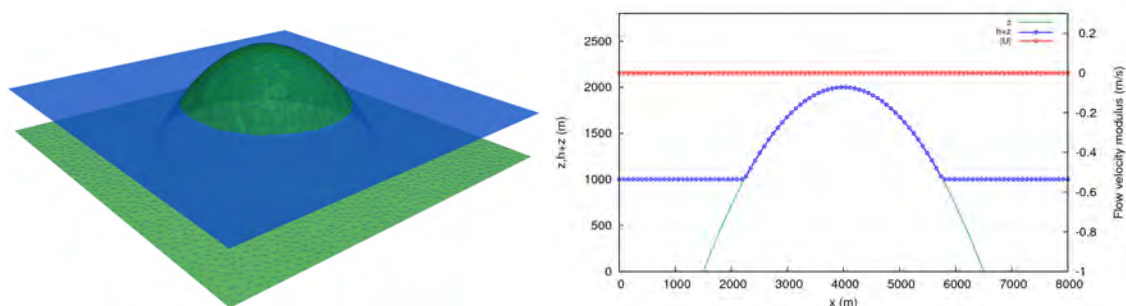
Figure 9: 3D representation of the steady state (left) and cross-sectional plot of the solution at the final time (right).
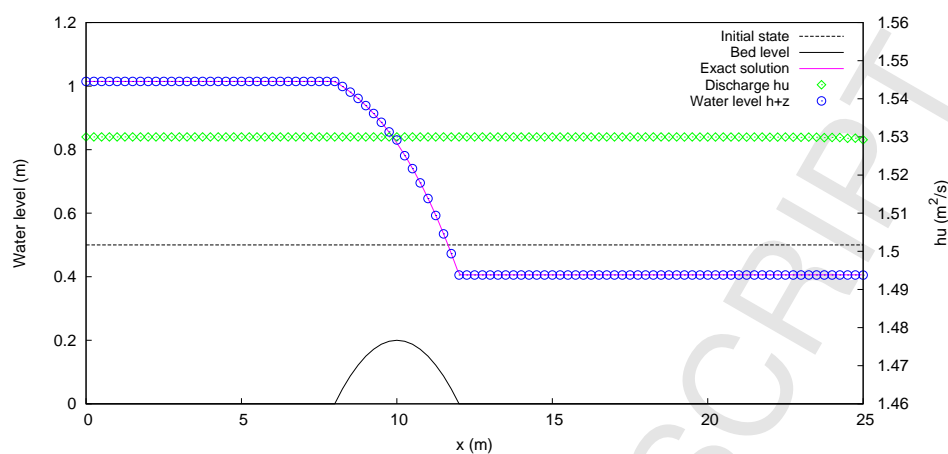
Figure 10: Numerical vs. exact solution for the steady state.
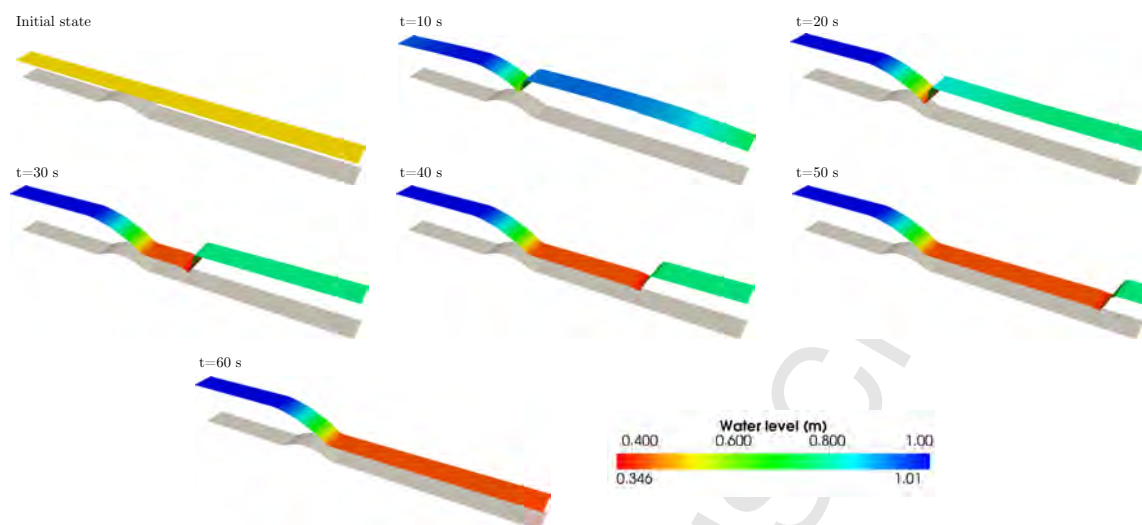
Figure 11: Convergence to the transcritical steady state over a bump.
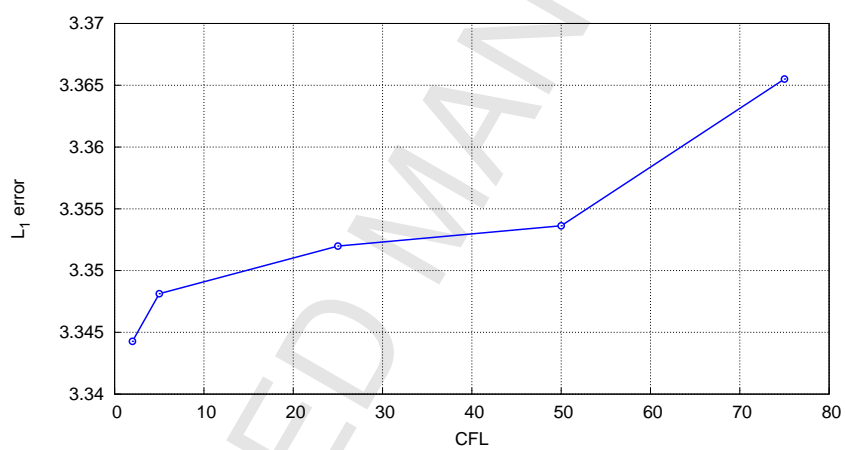
Figure 12: L_1 error with respect of CFL number.
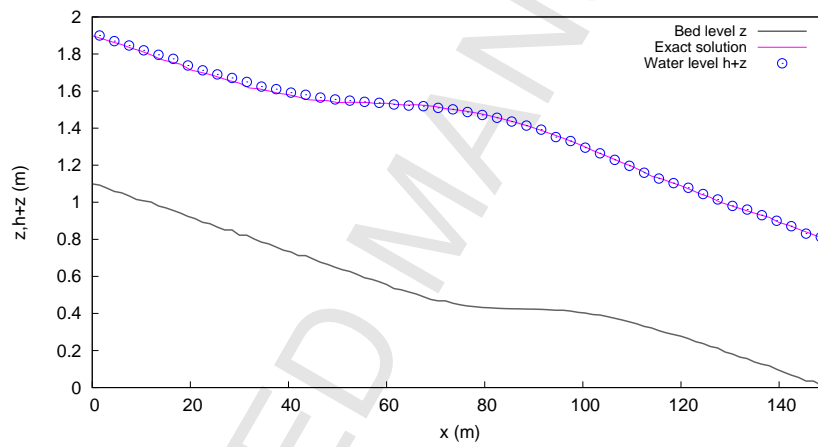
Figure 13: Comparison between numerical and exact solution for the MacDonald test case (CFL=300).
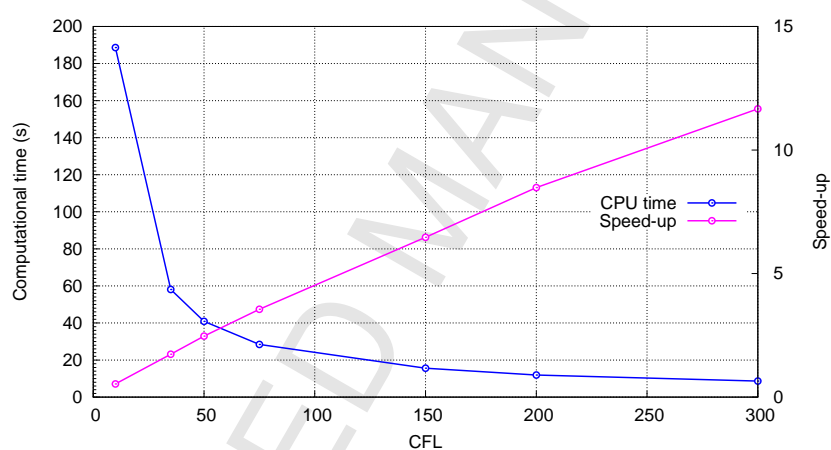
Figure 14: CPU times and speed-up values for the MacDonald test case.
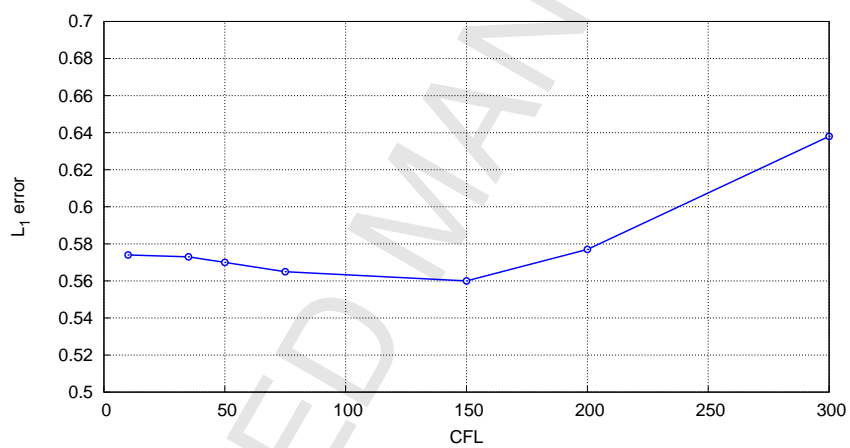
Figure 15: L_1 error with respect of CFL number.

46
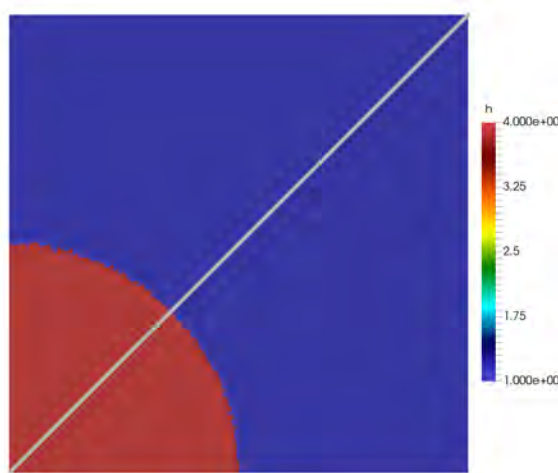
Figure 16: Initial conditions for the dam break test case and plotting line.
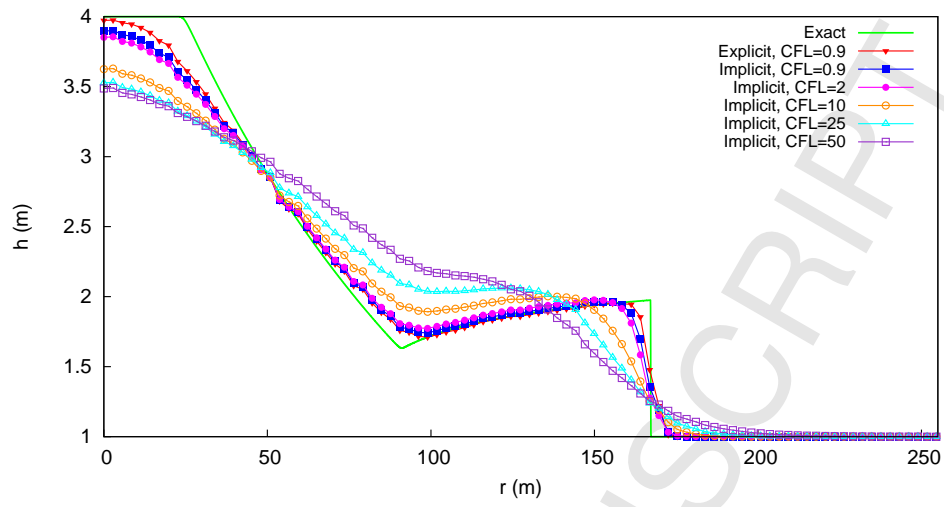
Figure 17: Numerical vs. exact solution for the dam break test case at $t = 12s$ (10363 cells mesh).
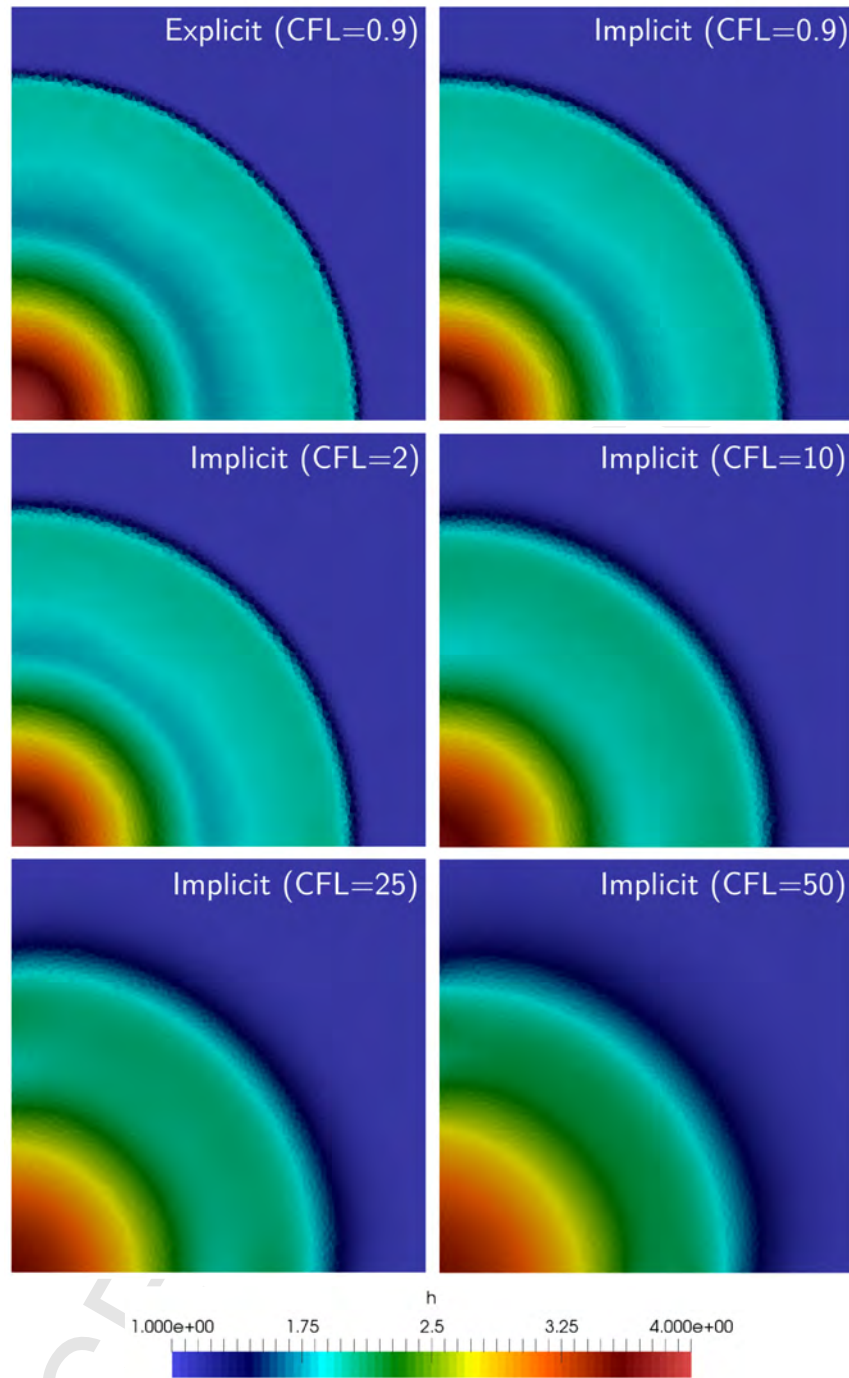
Figure 18: Transient solution for the circular dam break test case at $t = 12s$ for several CFL numbers (10363 cells mesh).
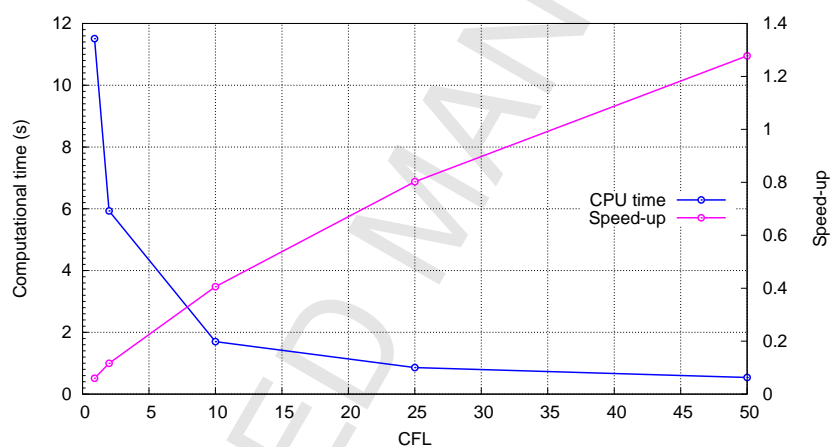
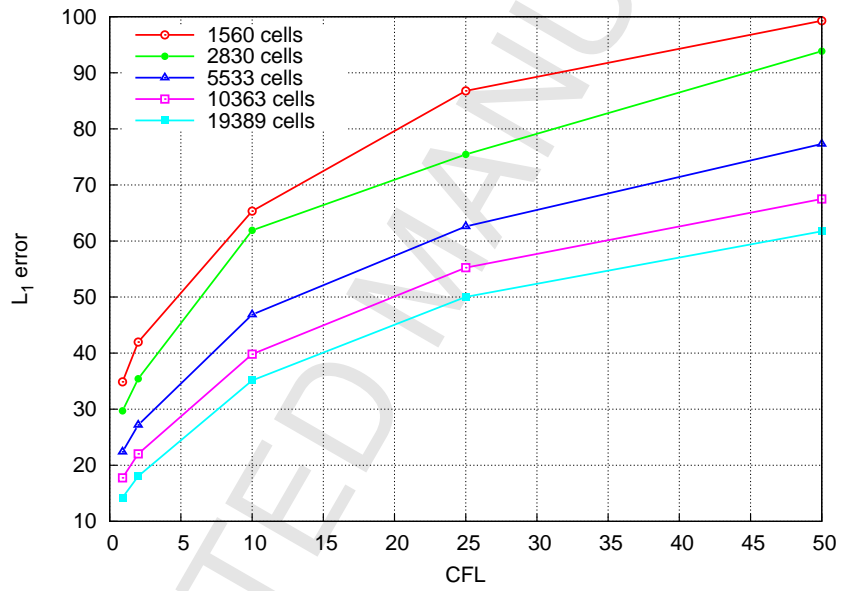Figure 19: CPU times and speed-up values for the circular dam break test case (10363 cells mesh).

49

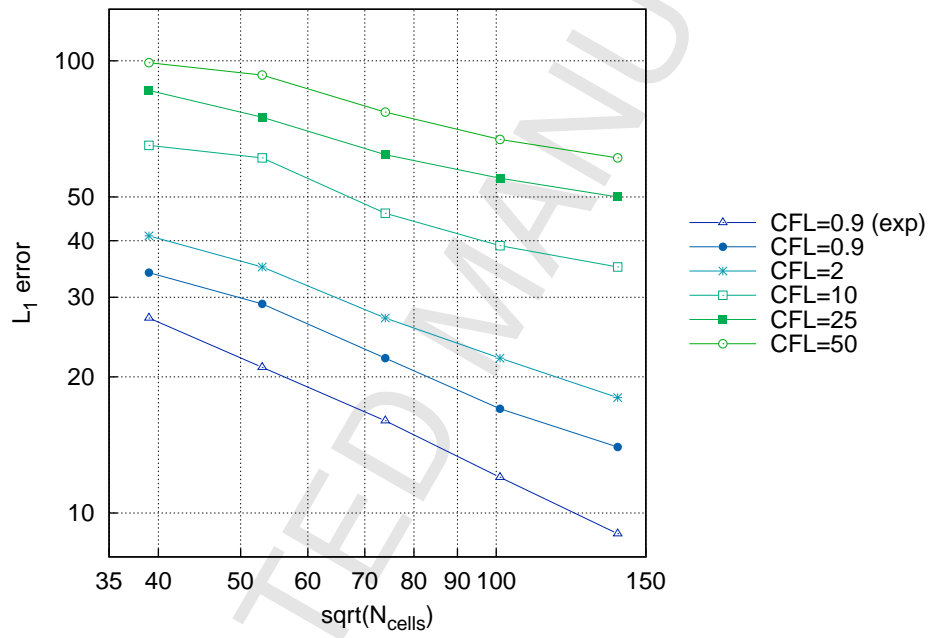Figure 20: L_1 error with respect of CFL number for several meshes.

Figure 21: L_1 error with respect of the mesh size in logarithmic scale for several CFL numbers.
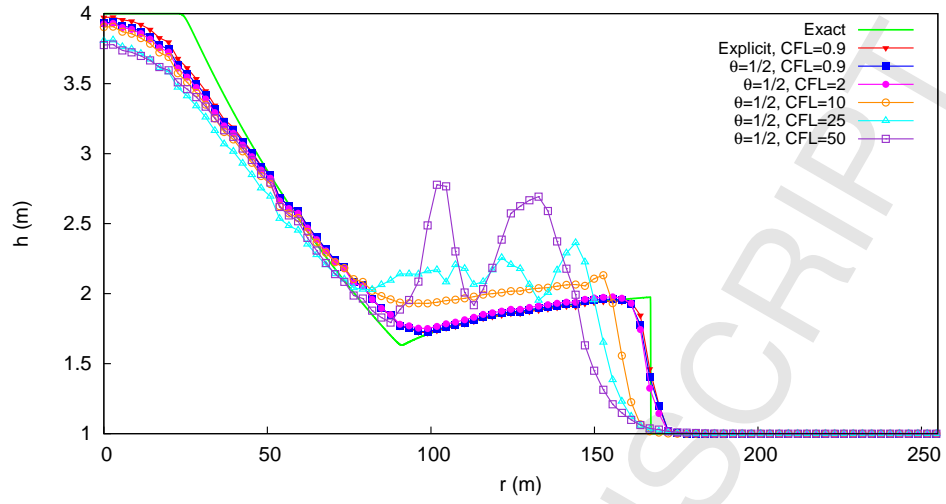
51

52

Figure 22: Numerical vs. exact solution for the dam break test case at $t = 12s$ using $\theta = 1/2$ (10363 cells mesh).
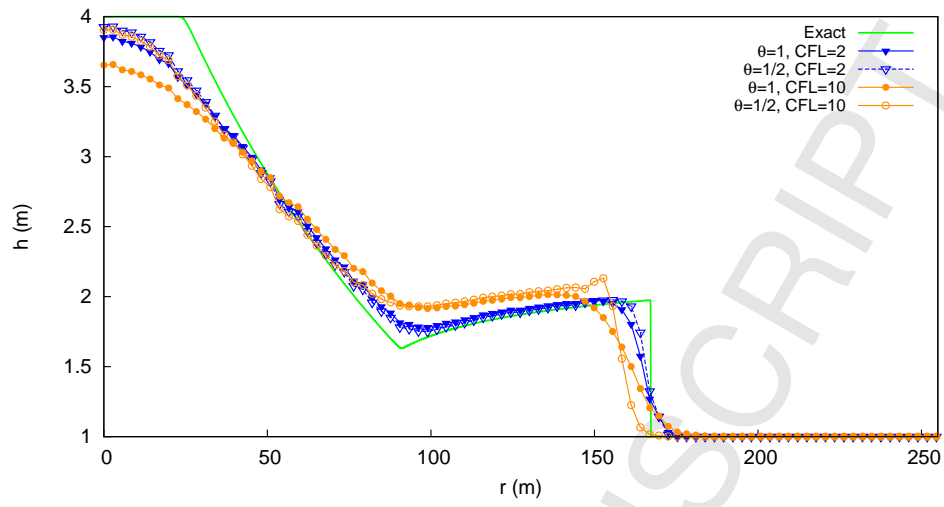
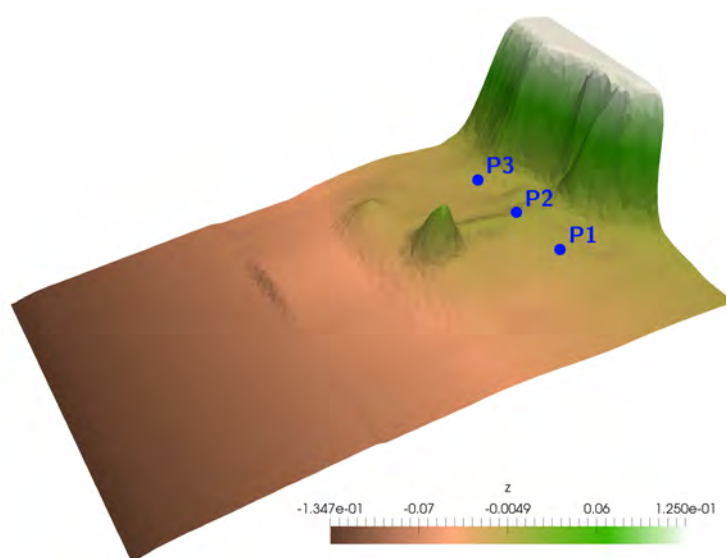Figure 23: Comparison between $\theta = 1$ and $\theta = 1/2$ numerical solutions (10363 cells mesh).

54

Figure 24: Tsunami test case topography and gauge locations.

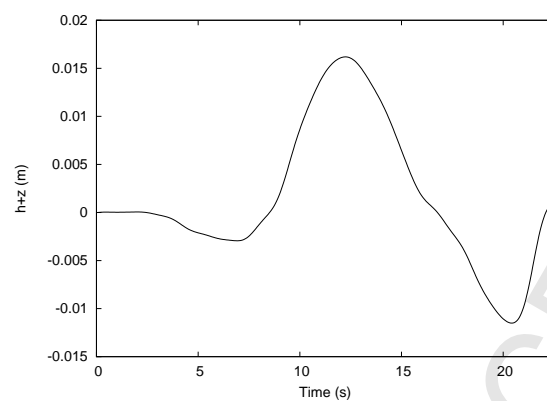Figure 25: Inlet boundary condition.

t=0

t=5 s

t=10 s

t=13 s

t=18 s

t=25 s

h

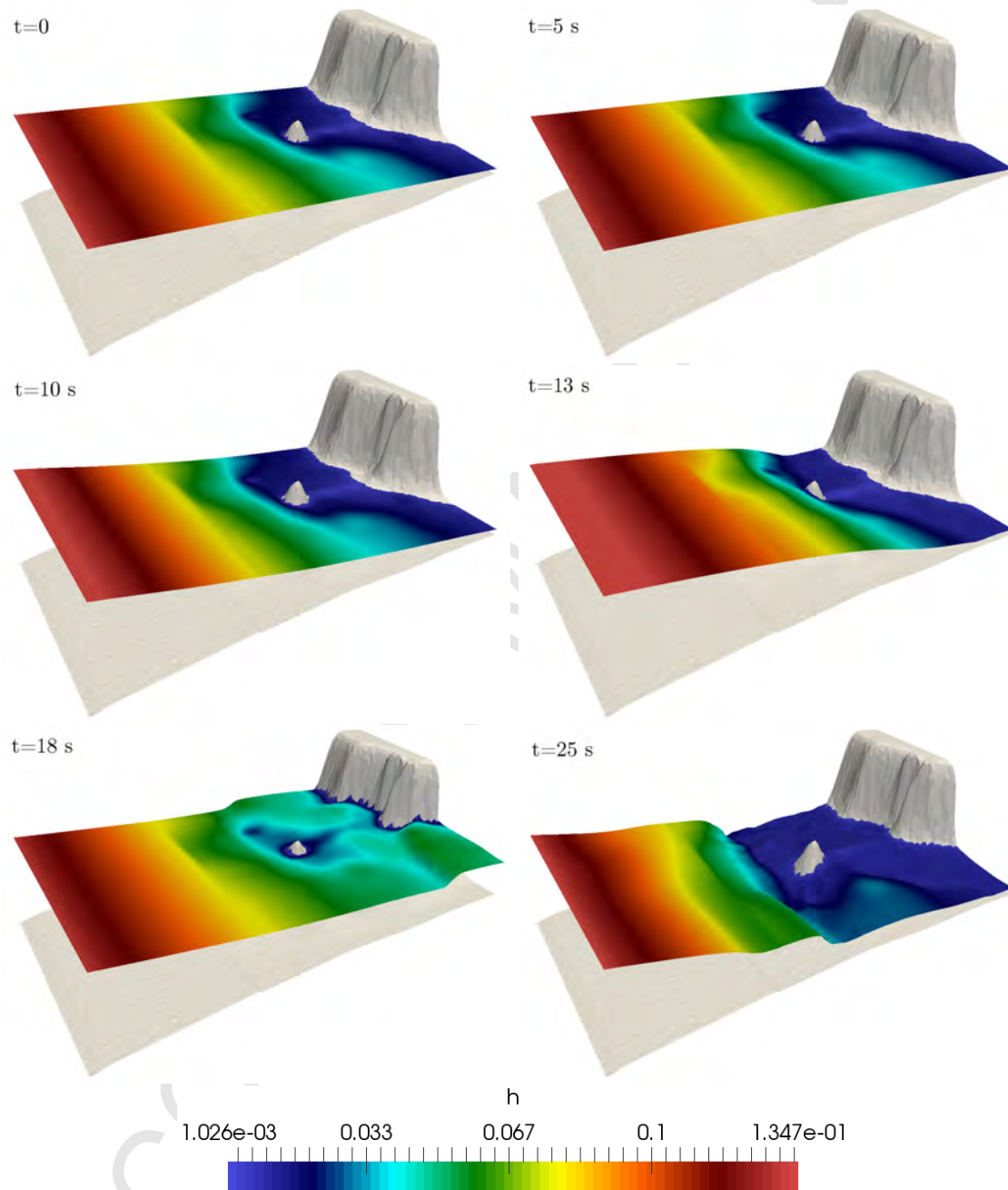1.026e-03   0.033   0.067   0.1   1.347e-01

Figure 26: 3D representation of the numerical results for water depth at several simulation times.
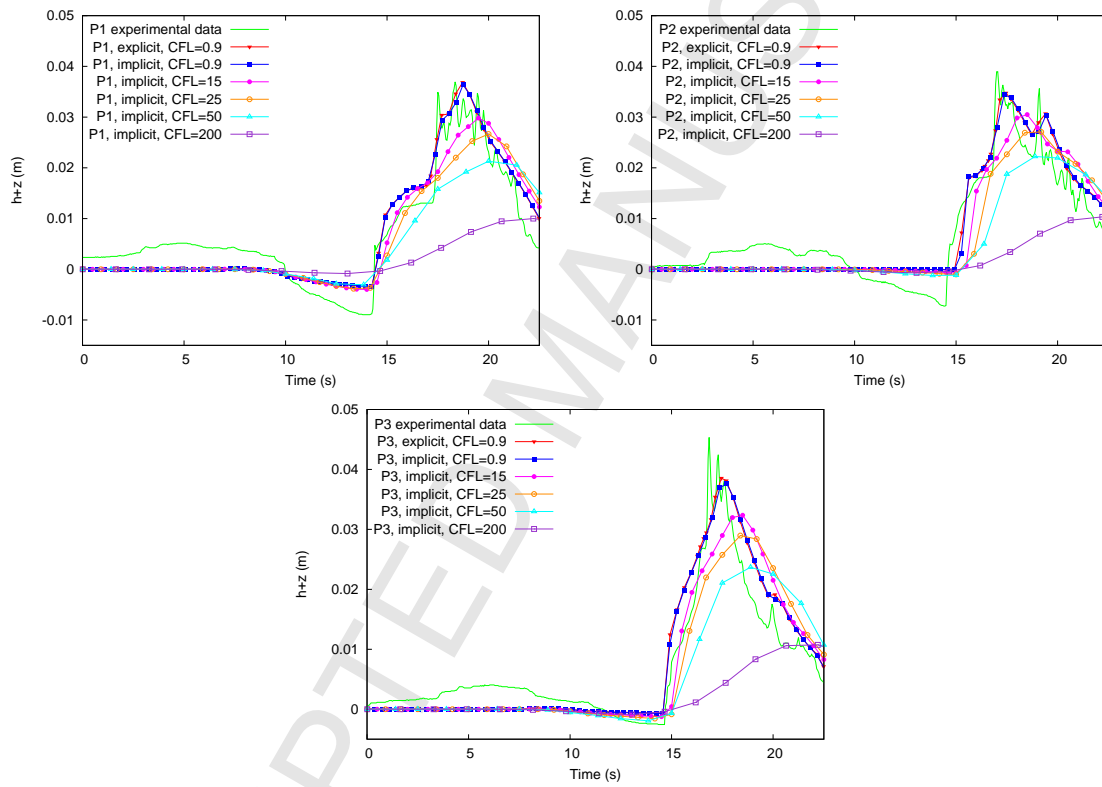
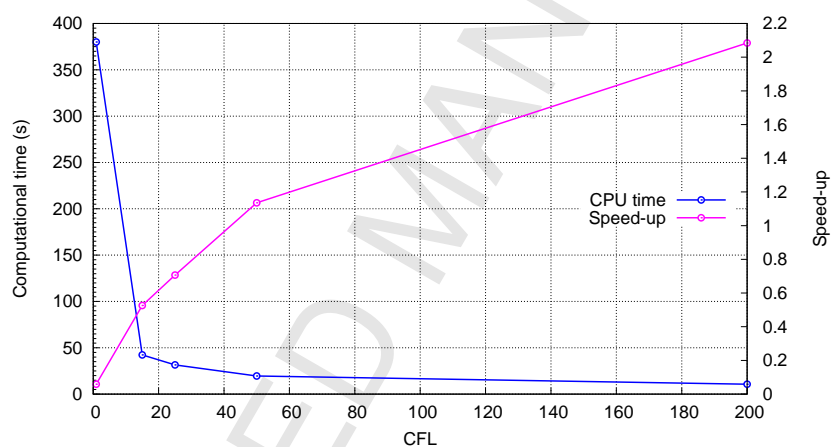Figure 27: Numerical results at the three gauging points.

Figure 28: CPU times and speed-up values for the tsunami test case.

Table 1: Transcritical test case L_1 errors in terms of the CFL number.

Scheme	CFL	L_1 error
Implicit	2	3.344
Implicit	5	3.348
Implicit	25	3.352
Implicit	50	3.354
Implicit	75	3.366

Table 2: MacDonald test case. CPU time, speed-up and L_1 error.

Scheme	CFL	CPU time	speed-up	L_1 error
Explicit	0.9	100.9	-	0.545
Implicit	10	188.6	0.53	0.574
Implicit	35	58.1	1.74	0.573
Implicit	50	40.9	2.47	0.570
Implicit	75	28.4	3.55	0.565
Implicit	150	15.6	6.47	0.560
Implicit	200	11.9	8.48	0.577
Implicit	300	8.65	11.66	0.638

Table 3: Circular dam-break test case. CPU time, speed-up and L_1 error.

N_{cells}	Scheme	CFL	CPU time	Speed-up	L_1 error
1560	Explicit	0.9	-	-	27.55
	Implicit	0.9	-	-	34.87
	Implicit	2	-	-	41.97
	Implicit	10	-	-	65.34
	Implicit	25	-	-	86.78
	Implicit	50	-	-	99.28
2830	Explicit	0.9	-	-	21.92
	Implicit	0.9	-	-	29.70
	Implicit	2	-	-	35.44
	Implicit	10	-	-	61.89
	Implicit	25	-	-	75.43
	Implicit	50	-	-	93.85
5533	Explicit	0.9	0.31	-	16.91
	Implicit	0.9	4.18	0.07	22.40
	Implicit	2	2.18	0.14	27.18
	Implicit	10	0.57	0.54	46.87
	Implicit	25	0.3	1.03	62.59
	Implicit	50	0.23	1.35	77.30
10363	Explicit	0.9	0.69	-	12.76
	Implicit	0.9	11.51	0.06	17.76
	Implicit	2	5.93	0.12	22.03
	Implicit	10	1.7	0.41	39.82
	Implicit	25	0.86	0.80	55.24
	Implicit	50	0.54	1.28	67.49
19389	Explicit	0.9	3.08	-	9.50
	Implicit	0.9	28.25	0.11	14.23
	Implicit	2	14.29	0.22	18.05
	Implicit	10	4.2	0.73	35.13
	Implicit	25	2.11	1.46	50.03
	Implicit	50	1.33	2.32	61.72

- We use a 2D implicit surface flow model based on shallow water equations.
- A robust wet/dry treatment is implemented.
- The scheme is validated by means of exact solutions and experimental data.
- CFL numbers up to 300 are reached.
- The efficiency of the implict scheme is explored.